

cf. 3



FUSK

**DEVELOPMENT PROGRAM FOR A
200 kW, CW, 28 GHz GYROKLYSTRON**

**H. Jory, C. Conner, S. Evans, J. Moran,
W. Sayer, D. Stone, R. Symons, G. Thomas**

FUSION ENERGY DIVISION LIBRARY
MAY 1980

**Quarterly Report No. 16
January through March 1980**

Prepared for:

**Oak Ridge National Laboratory
Oak Ridge, Tennessee 37830**

Operated by:

**Union Carbide Corporation for the Department of Energy
Contract No. W-7405-eng-26**

Varian Associates, Inc.
Palo Alto Microwave Tube Division
611 Hansen Way
Palo Alto, California 94303

DEVELOPMENT PROGRAM FOR A
200 kW, CW 28 GHz GYROKLYSTRON

H. Jory, C. Conner, S. Evans, J. Moran,
W. Sayer, D. Stone, R. Symons, G. Thomas

Quarterly Report No. 16
January through March 1980

Prepared for:
Oak Ridge National Laboratory
Oak Ridge, Tennessee 37830

Operated by:
Union Carbide Corporation for the Department of Energy
Contract No. W-7405-eng-26

Varian Associates, Inc.
Palo Alto Microwave Tube Division
611 Hansen Way
Palo Alto, California 94303

TABLE OF CONTENTS

<u>Section</u>		<u>Page No.</u>
I	INTRODUCTION	1
II	TECHNICAL DISCUSSIONS	3
	A. Tube 5R2	3
	B. Tube 7R1	21
	C. Tube 12(M)	21
	D. Tube #6	25
	E. Tubes #9 & 10	25
	F. Tubes #8 & 11	26
III	PROGRAM SCHEDULE AND PLANS	27
IV.	REFERENCES	30

LIST OF ILLUSTRATIONS

<u>Figure</u>		<u>Page No.</u>
1	Output Power vs Waveguide Length with 1.75 VSWR	4
2	Collector Power Dissipation	7
3	Magnetic Field Along Collector Axis for Three Values of Top Coil Current	8
4	Frequency & Power vs Main Magnet No. 2 Current for VGA-8000, S/N 5R2, $I_{\text{BEAM}} = 3.6 \text{ A}$	11
5	Frequency & Power vs Main Magnet No. 2 Current for VGA-8000, S/N 5R2, $I_{\text{BEAM}} = 4.9 \text{ A}$	12
6	Frequency & Power vs Main Magnet No. 2 Current for VGA-8000, S/N 5R2, $I_{\text{BEAM}} = 6.0 \text{ A}$	13
7	Efficiency vs Beam Current for VGA-8000, S/N 5R2 with Gun Anode Voltage Values Optimized for Peak Efficiency	14
8	Efficiency vs Gun Anode Voltage, $I_{\text{BEAM}} = 3.5 \text{ A}$	16
9	Efficiency vs Gun Anode Voltage, $I_{\text{BEAM}} = 5.0 \text{ A}$	17
10	Tube, Mode Filter and Miter Bend Configurations	19
11	VGA-8000 Gyrotron, S/N 12 Efficiency vs Beam Current in Pulse Mode; 8% Duty	22

ABSTRACT

The objective of this program is to develop a microwave oscillator capable of producing 200 kW CW power output at 28 GHz. The use of the gyrotron or cyclotron resonance interaction is being pursued.

During this reporting period the basic testing of axisymmetric tube 5R2 was completed. It successfully operated in excess of 200 kW both in pulse and CW modes. The measured power output of 212 kW establishes a new world record for CW power generation at 28 GHz. Further tests with various output guide components simulating the EBTS load were made.

Tube 7R1 (M) was returned to Palo Alto after operation ceased due to an open heater. It was replaced by tube 12 (M) which was tested to 113 kW CW and shipped to ORNL.

Construction of tube 6 was completed except for the collector seal and final assembly. A collector seal of a new design was constructed and is being evaluated.

Work on 5" axisymmetrical tubes, S/N 9 and 10, has been stopped with the intent of applying all remaining effort to the 2.5" axisymmetric tubes.

Construction of 2.5" axisymmetrical tubes 8 and 11 is progressing.

I. INTRODUCTION

The objective of this program is to develop a microwave oscillator capable of producing 200 kW of CW power at a frequency of 28 GHz. In addition, it is intended that the program will serve as the first step toward development of a device to produce a similar power level at a frequency of 60 and 110 GHz. Feasibility for the 60 and 110 GHz designs will be demonstrated, whenever practical, in the design of the 28 GHz device. Tunability or bandwidth is not considered an important parameter in the design, but efficiency is. Mode purity in the output waveguide is not a requirement for the device, but the circular TE mode is considered desirable because of its low loss properties.

With these objectives in mind, the decision was made to pursue an approach based on a cyclotron resonance interaction between an electron beam and microwave fields. The detailed arguments leading to this choice are contained in the final report of the preceding study program¹. The device configuration of particular interest, called a gyrotron, has been discussed in recent literature.^{2,3} It typically employs a hollow electron beam interacting with cylindrical resonators of the TE_{0m1} class.

The optimum beam for the cyclotron resonance interaction is one in which the electrons have most of their energy in velocities perpendicular to the axial magnetic field. Another requirement is that the small component of axial velocity be essentially the same for all electrons. An electron which has a different axial velocity will not interact efficiently. Generation of a beam with high transverse velocity and small axial velocity spread is another important design goal.

The approach chosen to generate the beam is a magnetron type of gun like the one used in the devices described in the Russian literature. With this type of gun, the shaping of the magnetic field in the gun region becomes quite important.

As a result of the excellent performance of the pulsed oscillator, producing up to 248 kW of peak power at 28 GHz with good efficiency⁴, the emphasis of the program has been shifted to stress the construction and delivery of CW oscillators.

During the period covered by this report, two CW tubes, S/N 5, an axisymmetric type, and S/N 12M, a miter-bend output type, were operated under pulse and CW conditions. A miter-bend tube, S/N 7M ceased to operate at ORNL and was returned to Palo Alto. Construction of three axisymmetric tubes; S/N 6, 8, and 11 was continued. Work on the 5" axisymmetric tubes S/N 8 and S/N 11 was discontinued.

The following observations on these tubes are reported here in the order in which they were tested or assembled.

II. TECHNICAL DISCUSSIONS

A. Tube 5R2

Pulse processing of this tube continued in early January until a peak power of 213 kW at 10% duty was achieved. Some difficulty was experienced at turn-on due to a tendency to oscillate at 32.5 GHz and 33.2 GHz. However, by careful adjustment of main field magnet #2 current and modulation anode voltage, a technique was worked out for turning on the tube.

Following this, a single miter-bend was inserted between the waterload and the tube output. The mismatch caused by this was severe enough to prevent operation in the normal 27.9 GHz mode. The tube showed a strong tendency to oscillate at 26.8 GHz. A conduction cooled mode filter was then inserted between the tube output and the miter-bend, whereupon the tube operated in its normal mode.

The miter-bend and mode filter were then removed and a Teflon disc with a VSWR of 1.75 was inserted between the tube and the rf load and a study of its effect on output power as a function of line length was made. The line was lengthened in $.28 \lambda$ increments. This data, plotted in Figure 1, shows an approximately $\pm 11\%$ peak-to-peak power variation.

The test set was then converted to CW operation and processing and testing continued. As the collector power was steadily increased, a tendency for increased body current was noted at a beam voltage of 60 kV. A body current as high as 25 milliamperes was recorded compared to a typical value of 10 milliamperes. However, at 80 kV the body current had decreased to a normal 18 milliamperes. A possible explanation for this is that an oscillation had occurred under the aforementioned conditions. This phenomenon was noted on several occasions but caused no apparent harm to the tube.

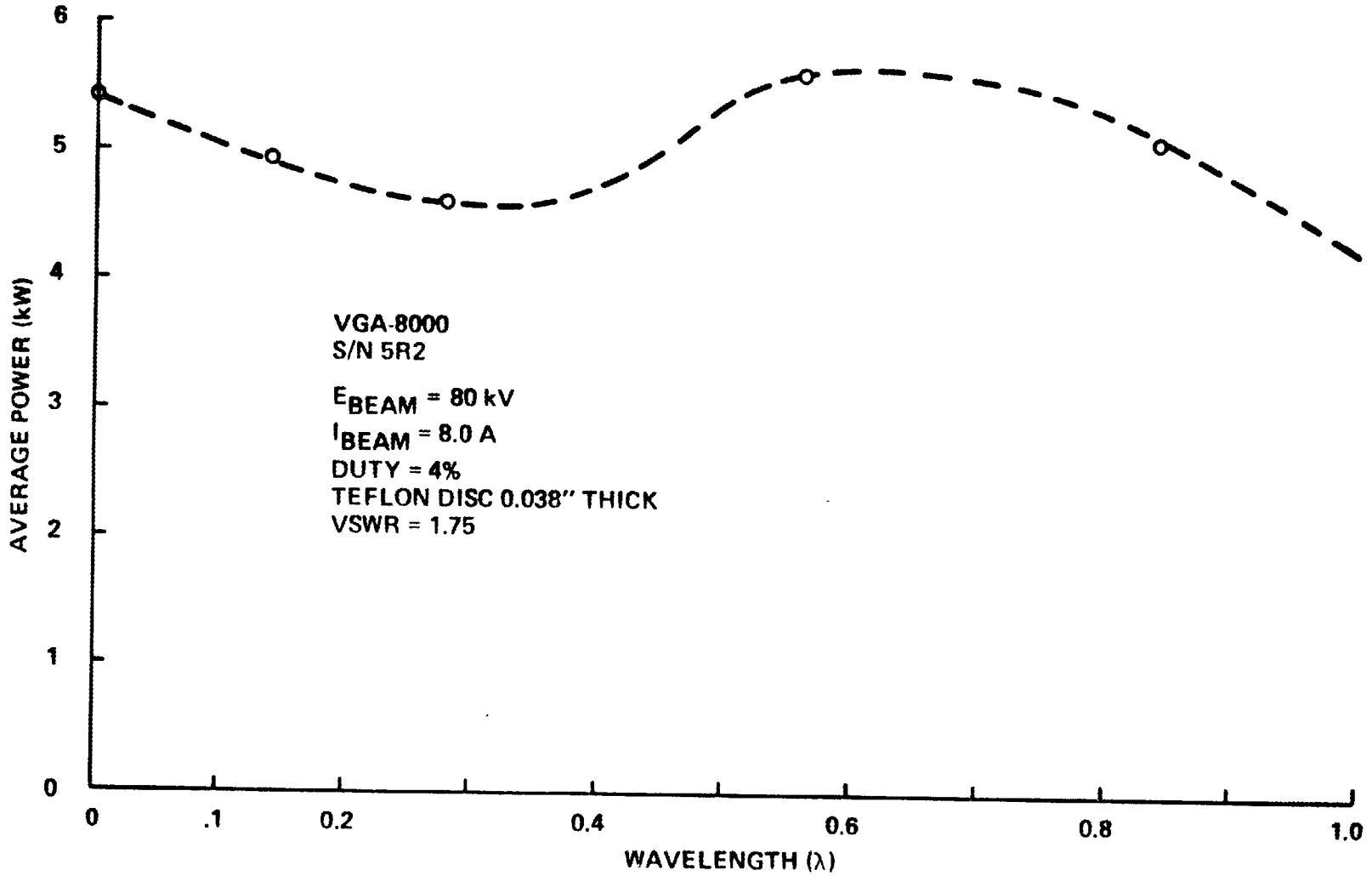


Figure 1. OUTPUT POWER vs WAVEGUIDE LENGTH WITH 1.75 VSWR

Processing continued and the tube was successfully tested at 60 kW CW for 12.5 hours, 100 to 108 kW CW for 3.4 hours and 140 kW CW for 2.3 hours. Two hours of the 140 kW CW operation proceeded uninterrupted. During this process a differential temperature rise of 3 to 8 degrees C was noted in the collector seal which depended upon the rf level. Temperature decreased as the rf level was increased. Upon further investigation, this was found to be related to the top collector coil current and is believed to have been caused by interception of the beam near the collector seal. In order to better understand this, the electron beam power density on the collector walls was investigated.

The total collector surface area is determined by the limits of the thermal design. State of the art collectors of this type are capable of reliably handling up to $\sim 1 \text{ kW/cm}^2$ of beam power density. Any thermal loading in excess of this level greatly increases the risk of catastrophic collector failure during tube operation.

Subject to this upper limit in power density, the collector dimensions are the result of a compromise between excessive collector mode trapping and impractical tube length. In order to alleviate the problem of mode trapping, it is necessary to minimize the collector radius and thus limit the number of waveguide modes which can propagate in the collector. As there is a minimum collector surface area allowed, the collector radius may be reduced only at the expense of increased collector length. The region of electron collection may be lengthened by magnetically spreading the spent electron beam over a region which is consistent with the upper limit in collector wall power density and does not lead to an impractical collector length. The most critical thermal loading occurs when operating at full beam power (640 kW CW) without rf oscillation. (Thermal loading due to rf dissipation at the collector walls is negligible in comparison to the beam thermal loading.) The collector is designed for this worst case.

A substantial safety margin is built into the design to allow for the changes in beam dynamics and concomitant changes in beam position and thermal loading which occur when the tube is brought into oscillation. During rf operation the electron dynamics change for two reasons. First,

the gyrotron interaction depletes the electrons' perpendicular energy, leading to a shift in thermal load toward the output end of the collector. This energy depletion depends on the interaction efficiency encountered at the operating point, and as the tube is brought into oscillation a large range of operating parameter space is sampled. Thus, the interval of tube "turn-on" is accompanied by significant variations in power deposition in the collector. Second, the rf fields in the output waveguide can further retard or accelerate a small fraction of the beam electrons. This effect is noteworthy in that the presence of any highly energetic electrons in the collector poses the danger of electron puncture of the output window ceramic. This problem is solved by placing transverse magnets between the collector and the output window.

The effectiveness of magnetic contouring of the electron beam power density on the collector walls has been confirmed with x-ray measurements. The hard target x-ray bremsstrahlung flux was observed outside the collector as a function of axial position. The measurements were made by exposing medical x-ray film (Kodak type AA) to the x-ray flux for 10 minutes at one half of full beam power (320 kW CW) with the tube out of oscillation. The resulting x-ray intensity data have been converted to collector wall power density by a suitable normalization of the data to the available beam power, and are shown in Figure 2. The three curves represent three values of current in the top collector magnet coil, specifically 0.5, 0.75, and 1.0 A. The most sharply peaked curve (a), when scaled up by a factor of two for operation without rf at full beam power, reaches a peak value of 680 kW/cm^2 . A less demanding power density curve (b) is achieved by increasing the top collector coil current by 50%. A further increase in the top collector coil current produces the flat curve (c). The latter case is expected to be skewed still further toward the output window when the tube is brought into oscillation, and for this reason the second curve was chosen as the ideal operating point for collector loading.

To compare with the results of the x-ray analysis, magnetic field profiles were plotted for three magnetic field settings. Figure 3 shows the magnetic fields for the bottom coil set at 2A, the middle coil at 2A, and the top coil varied between 0.5 A, 0.75 A, and 1 A. Using these magnetic

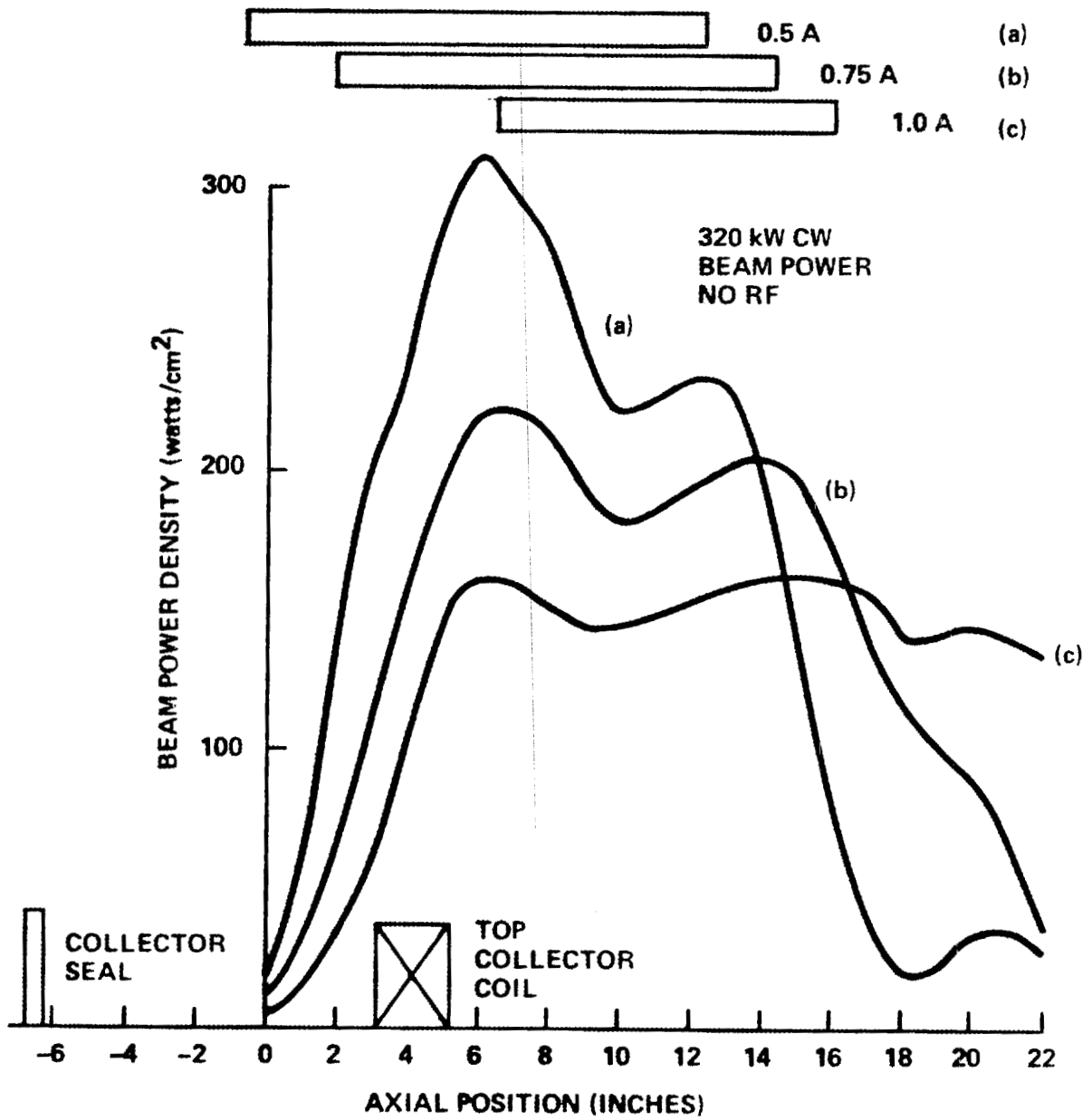


Figure 2. COLLECTOR POWER DISSIPATION

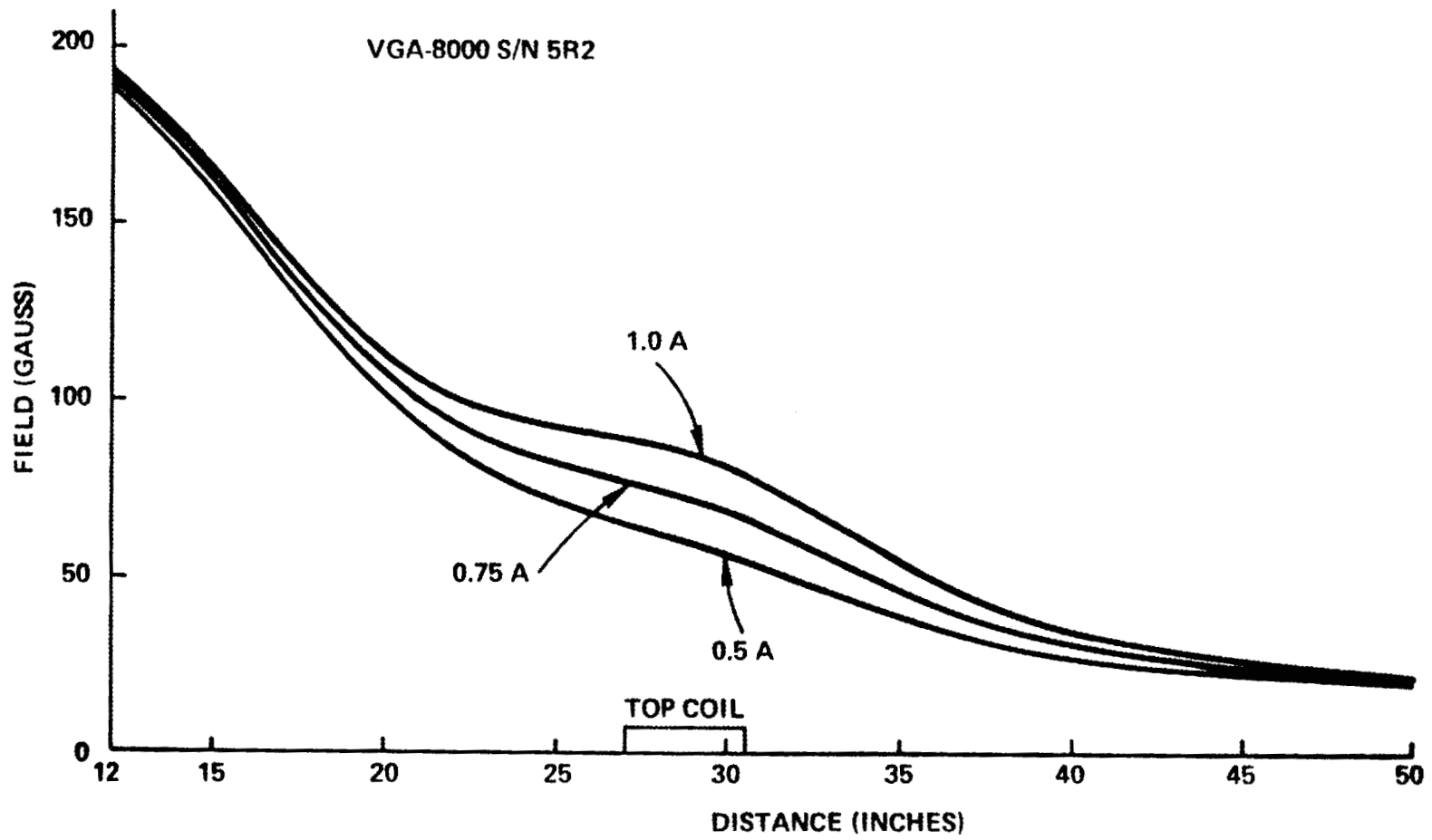


FIGURE 3. MAGNETIC FIELD ALONG COLLECTOR AXIS FOR THREE VALUES OF TOP COIL CURRENT

field measurements, we have calculated the axial location of the electron collection region (indicated by the horizontal base (a), (b), and (c) in Figure 2) by assuming that the beam expands adiabatically in the collector. While a stronger magnetic field shifts the electron beam further down the collector as expected, the simple adiabatic calculation provides only a crude description of the region of electron beam impact. Notice that with increasing magnetic field strength, the electron beam intercepts further down the collector (Figure 2). The 0.5 A case shows the electron beam intercepting close to the collector seal. This case was the original setting used in CW operation and seems to correlate with the collector seal heating. The 1.0 A case shows a high level of electrons at the end of the collector - not a good situation. Consequently, the middle case with 2A on the bottom coil, 2 A on the middle coil, and 0.75 A on the top coil was chosen.

Although there is no quantitative data; qualitatively, the amount of collector seal heating appeared to decrease with the 0.75 A setting. Another advantage to the 0.75 A setting is the more even distribution of electrons through the collector. Thus, collector power density is kept lower with the 0.75 A setting compared to using 0.5 A on the top coil.

CW operation and processing of tube 5R2 continued. After consultation with Oak Ridge, differential thermometers were installed on the collector seal water and the window FC75 coolant flow inlets and outlets. This greatly improved the accuracy of measuring power dissipation in these critical assemblies. Power output was then gradually increased and the tube operated for several hours at intermediate power levels until 212 kW CW was achieved at 41% efficiency. At the 212 kW output level, power dissipation in the FC 75 window coolant and collector seal was found to be 1128 watts and 376 watts respectively. Table 1 is a summary of the final test performance and the related major parameter values.

The tube still had a tendency to oscillate in the 32.5 GHz during turn-on, similar to behavior in the pulse mode described earlier. By

Careful adjustment of the gun and main magnet coils, operation at 32.5 GHz was minimized and the tube operated easily from turn-on at 20 kW up to 212 kW CW.

A series of CW experiments was conducted in an effort to characterize the VGA-8000 gyrotron, as well as to better understand gyrotron operation. Three curves of power and frequency versus main magnet coil #2 for beam currents of 3.6 A, 4.9 A, and 6.0 A are shown. (Figures 4, 5, and 6.) Note that main magnet coil #2 is located toward the output end of the interaction cavity.

Close examination of these three curves shows some important trends. First, there is a value of magnetic field for peak output power. This value of magnetic field decreases with increasing beam current. Second, the frequency decreases markedly with decreasing coil #2 current. Both of these trends are typical of gyrotron operation.

Efficiency versus beam current with optimized gun anode voltage was plotted to provide insight into optimal operation. (Figure 7.) The peak efficiency observed was 48.7% at 3.5 A of beam current. As the beam current was increased a slight decrease in efficiency was noted. However, two important points are worth consideration. First, the efficiency values for beam currents greater than 5.2 A were obtained with slightly lower gun anode voltages; i.e., there is a possibility of higher efficiencies with increased gun anode voltage if the self-imposed safety limitation of 200 kW CW could be exceeded. Second, the efficiency values for beam currents less than 5.2 A were obtained before correcting the main magnetic field for optimal operation. Consequently, the efficiency for beam currents less than 5.2 A are also somewhat understated.

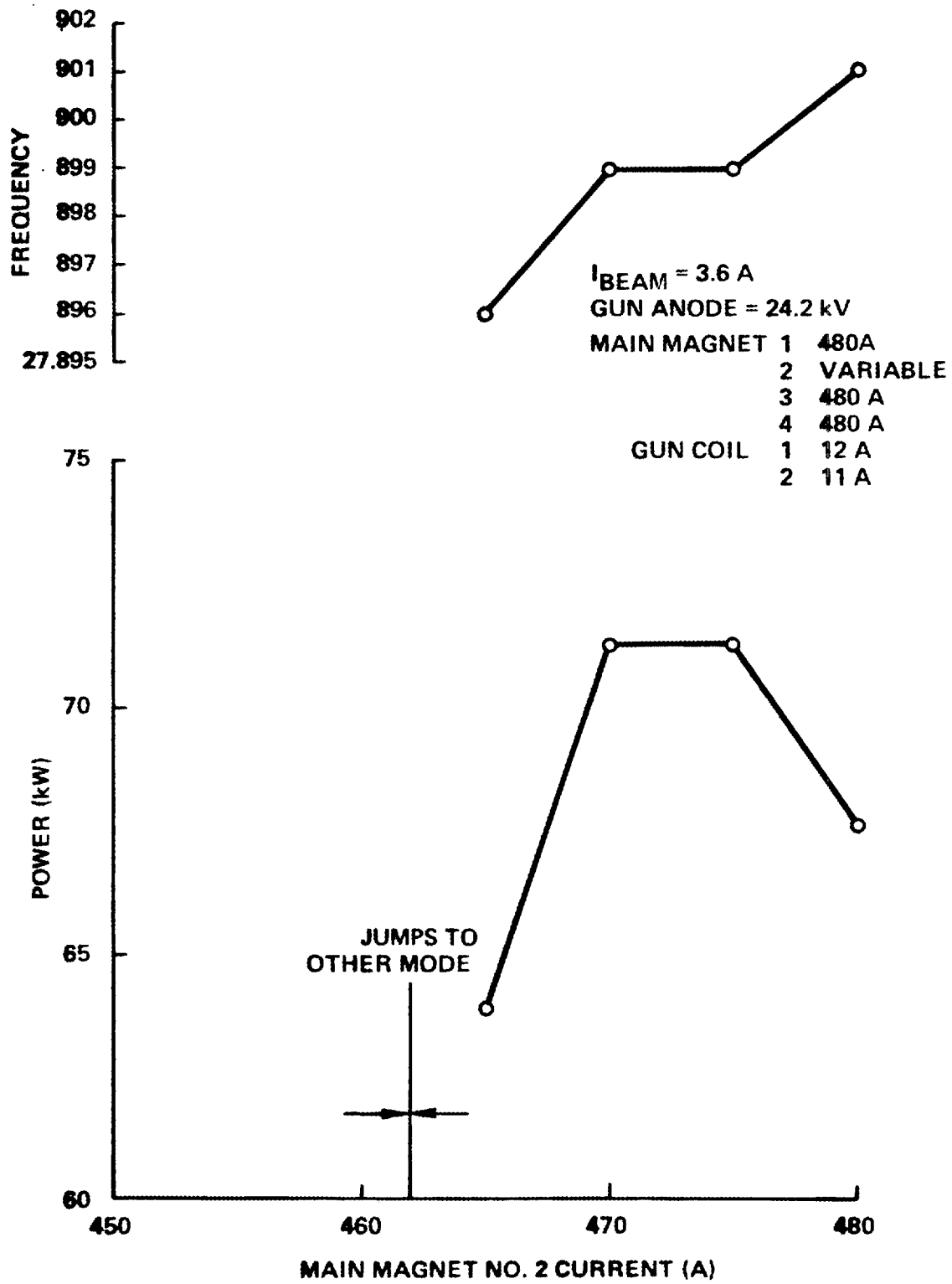


FIGURE 4. FREQUENCY & POWER VS MAIN MAGNET NO. 2 CURRENT FOR VGA-8000, S/N 5R2

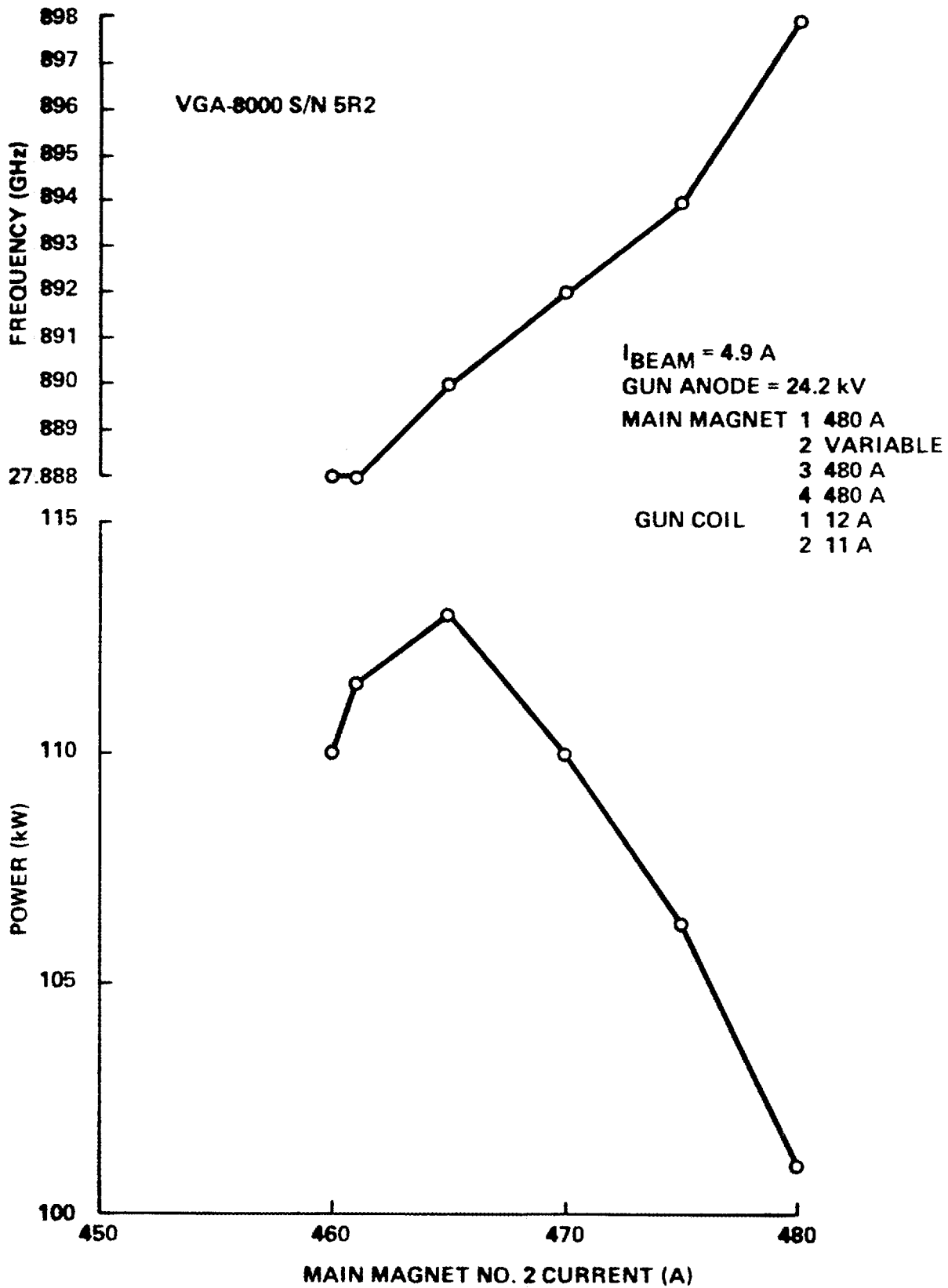


FIGURE 5. FREQUENCY & POWER VS MAIN MAGNET NO. 2 CURRENT FOR VGA-8000, S/N 5R2

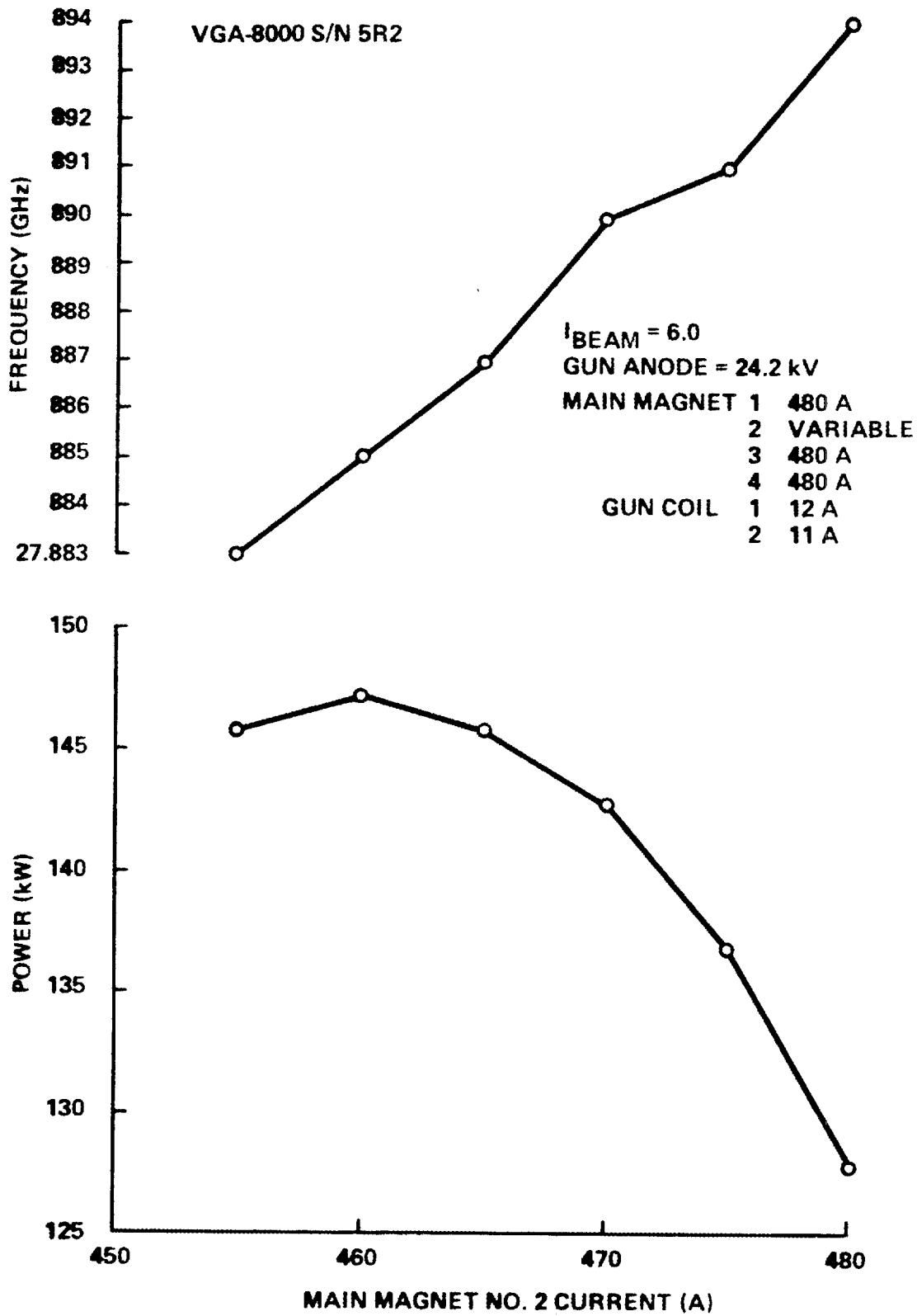


FIGURE 6. FREQUENCY & POWER VS MAIN MAGNET NO. 2 CURRENT FOR VGA-8000 S/N 5R2

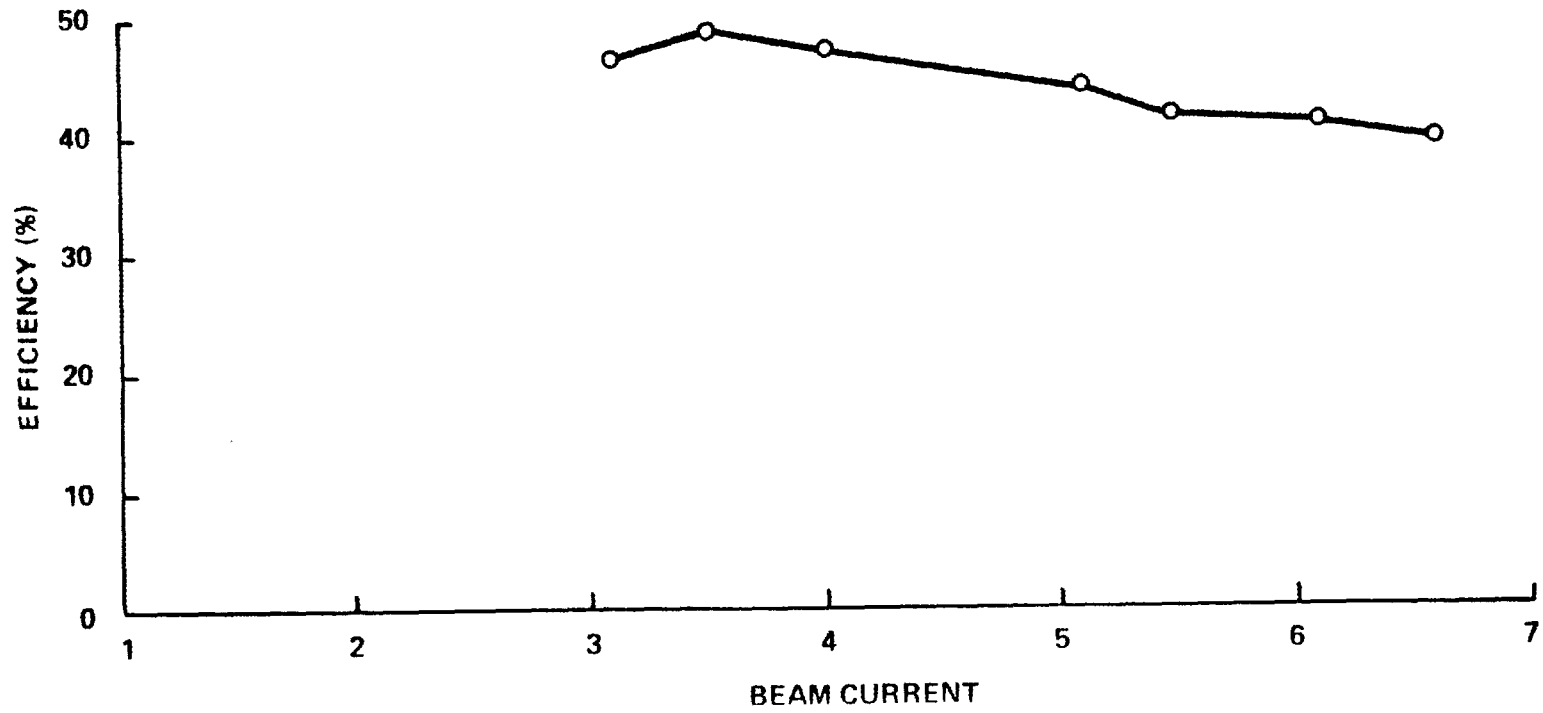


FIGURE 7. EFFICIENCY VS BEAM CURRENT FOR VGA-8000, S/N 5R2 WITH GUN ANODE VOLTAGE VALUES OPTIMIZED FOR PEAK EFFICIENCY

Table 1
VGA-8000 S/N 5R2 Test Performance

OPERATING PARAMETERS

Collector Water Flow	261 gpm
Body Water Flow	3.6 gpm
Window Water Flow (both)	1 gpm
FC-75 Flow	3.0 gpm
Collector Seal Flow	2.5 gpm
Magnet Coil Currents:	Main 1 = 475 A
	2 = 469 A
	3 = 460 A
	4 = 478 A
	Gun 1 = 12.5 A
	2 = 11.0 A
Beam Voltage	80.2 kV
Gun Anode Voltage	25.3 kV
Cathode Current	6.7 A
Body Current	25 mA
Heater Voltage	10.8 V
Heater Current	6.03 A
Power Output	212 kW
Frequency	27.870 GHz

Two curves of efficiency versus gun anode voltage were plotted (Figures 8 and 9). Figure 8 is a curve of efficiency versus gun anode voltage at 3.5 A of beam current. As shown, the efficiency increases almost linearly or slightly exponentially with gun anode voltage. The peak efficiency of 48.7% occurs at 26.8 kV. The curve suggests that efficiency continues to increase

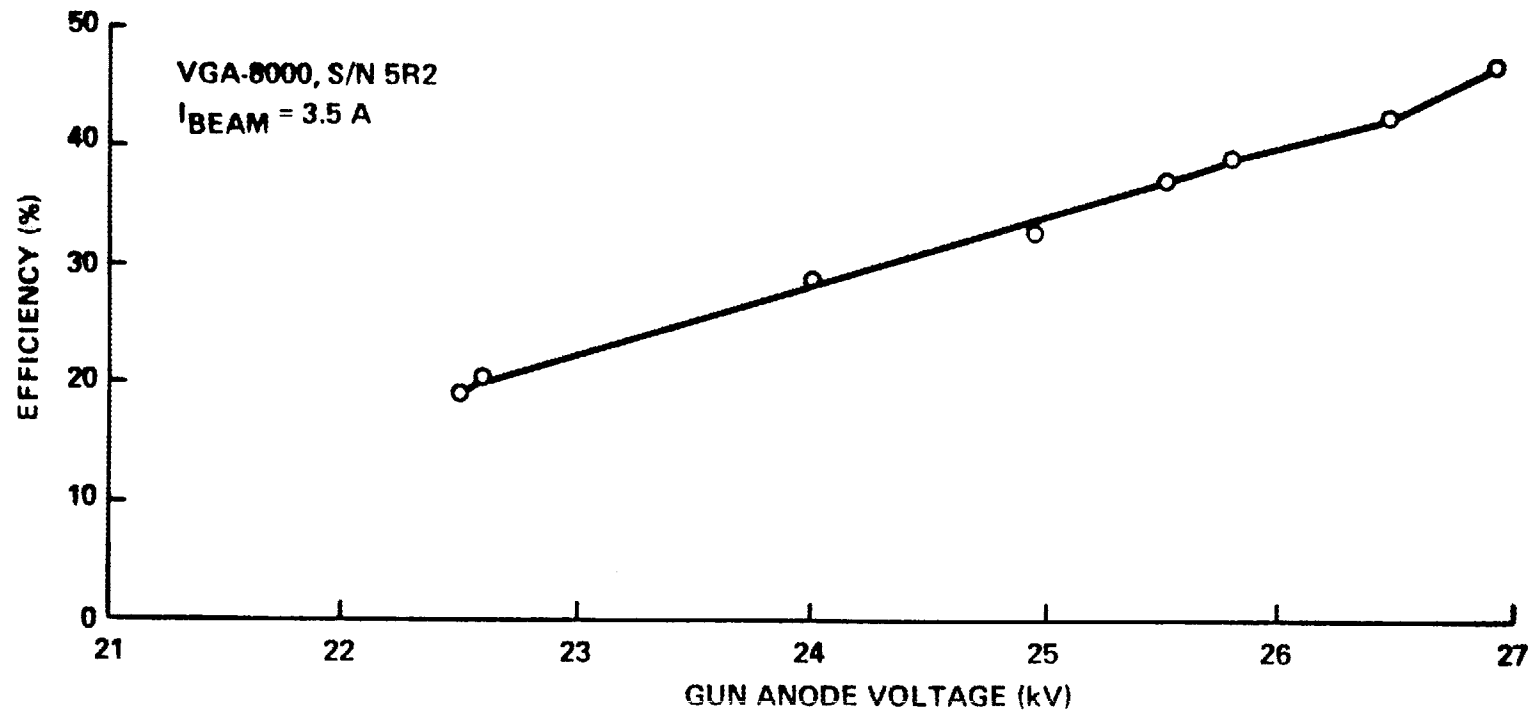


Figure 8. EFFICIENCY vs GUN ANODE VOLTAGE

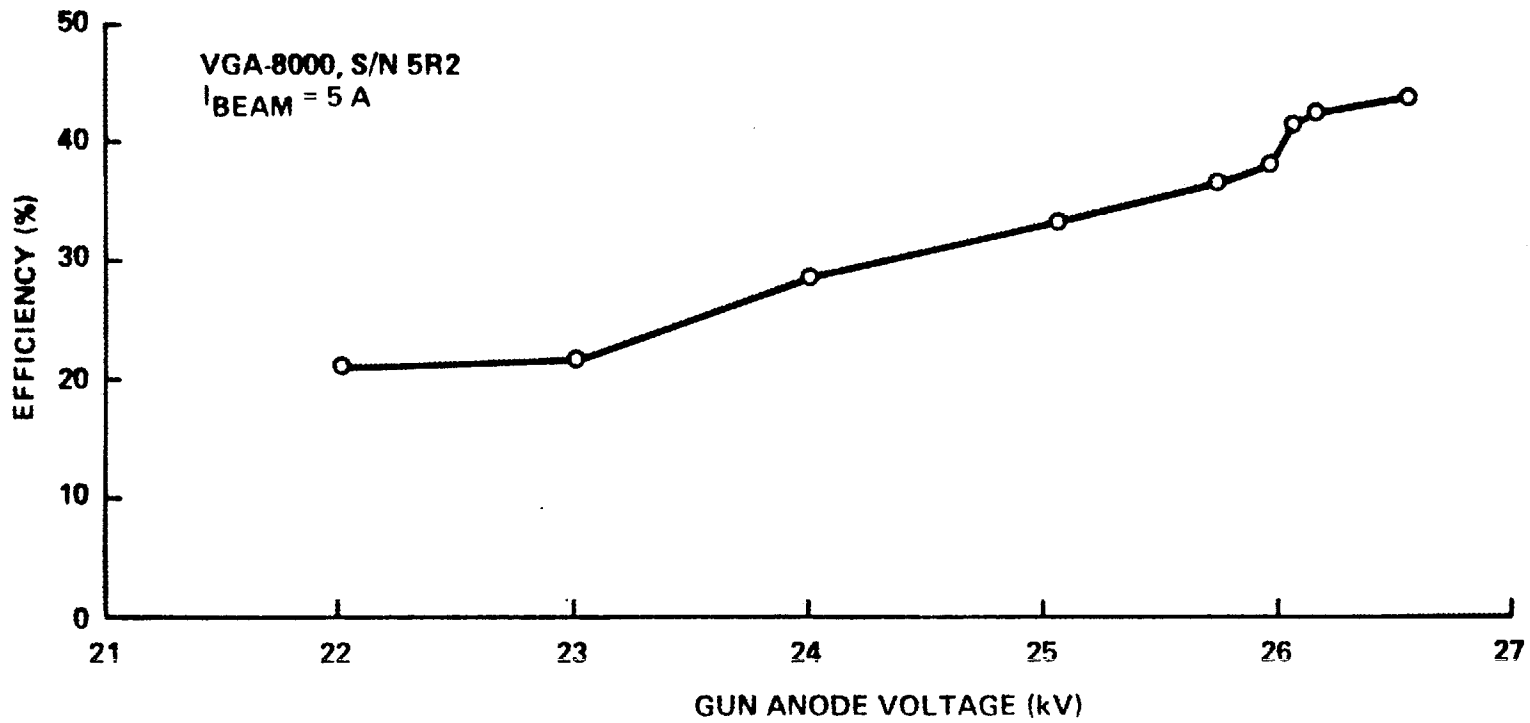


Figure 9. EFFICIENCY vs GUN ANODE VOLTAGE

above 26.8 kV. However, this is not the case. Above 26.8 kV the gun anode begins to draw current due to beam interception preventing any further increase in efficiency.

At 5 A of beam current, the efficiency versus gun anode voltage curve (Figure 9) shows similar characteristics as the curve for 3.5 A. The "kink" in the curve between 26 kV and 26.25 kV is due to a nonoptimized main magnetic field. Another problem due to nonoptimization of magnetic field was that the gun anode began drawing current at a lower gun anode voltage. This current prevented increasing gun anode voltage and thus limited the ability to achieve higher efficiency.

The tube was returned to pulse operation at 4% duty. The principle reason for this was to determine the performance of the tube with various combinations of miter-bends and mode filters as a means of better understanding its performance when coupled with the EBTS.

The 28 GHz gyrotron was first operated into a mode filter (Varian VFA-8000) and waterload. (Figure 10A.) Approximately 0.8% of the total power was absorbed by the mode filter with the remaining 99.2% absorbed in the waterload.

The second test was with a gyrotron operated into a mode filter, a miter bend, and the waterload. (Figure 10B.) The miter bend is a simple 45° plane surface reflector. Approximately 2.8% of the total power was absorbed in the mode filter and 97.2% was absorbed by the load.

Test three consisted of the tube, two mode filters, a miter-bend and the waterload. (Figure 10C.) The power absorbed in mode filter #1 (closest to the gyrotron) was 1.4%, with 2.50% in mode filter #2, and 96.1% in the load.

Test four involved operating the gyrotron into mode filter #1, a miter-bend, mode filter #2, another miter-bend and the waterload. Three different radial orientations of the second miter with reference to the first were tried with varying results. For the up-over-up orientation

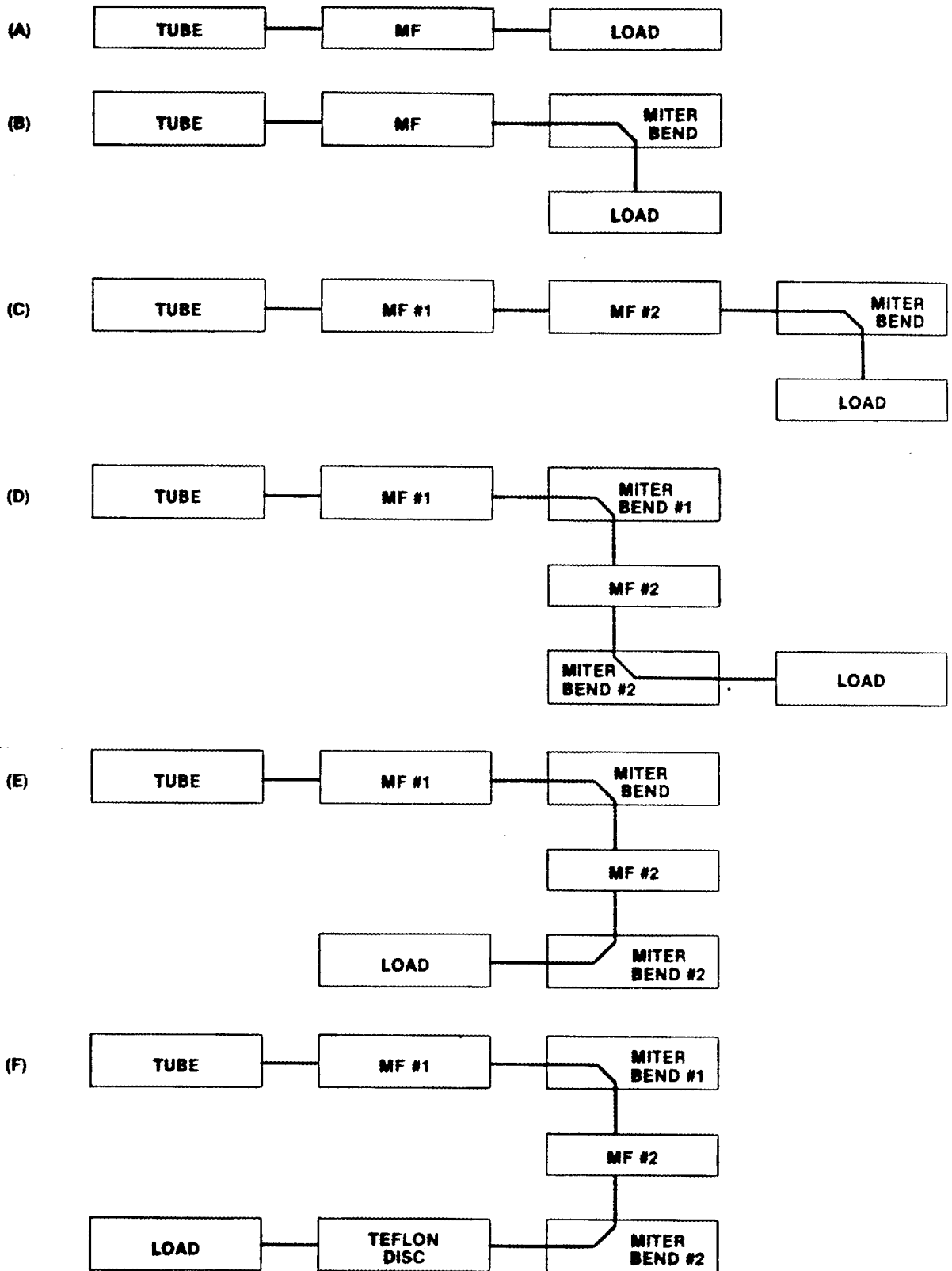


FIGURE 10. TUBE, MODE FILTER AND MITER BEND CONFIGURATIONS

(Figure 10D), mode filter #1 absorbed 4.3% of the total power, mode filter #2 absorbed 5.5% with 90.2% in the load. In this test, no attempt was made to determine the amount of power reflected back into the gyrotron. For the up-over-down orientation used at Oak Ridge (Figure 10E), mode filter #1 absorbed 6.73%; mode filter #2, 9.38% and the waterload, 83.89%.

The final orientation was up-over-up (Figure 10D) with the second miter tilted 45° from vertical. Mode filter #1 absorbed 4.73%, mode filter 2, 5.71% and the waterload, 89.56%.

Assuming a mode filter absorbs all non-circular electric modes, from the results of the first test, the minimum percentage of all non-circular modes in the gyrotron output power is 0.8%. From test results on miter bend gyrotron S/N 12, the mode filter was found to absorb approximately 4.7 dB or 66% of all non-circular power. Therefore, with this assumption, the percentage of all non-circular gyrotron output power is $0.8/0.66 = 1.2\%$. Thus, 98.8% of the output power is in one or more circular electric modes.

The data taken in tests two through five and measurements planned for tube S/N 6 will be studied further. An effort will be made to establish the effect of miter bends on the circular and non-circular mode content of the forward, reflected and mode converted power in the system for inclusion in a subsequent report.

In an effort to approximate the EBT load, a Teflon disc was placed in the output waveguide directly before the waterload. (Figure 10F.) The complete set-up was as follows: the gyrotron, mode filter, #1, a miter-bend, a mode filter, #2, a miter-bend, the Teflon disc, and the waterload. 0.28λ thick spacers were used to change the line length from the gyrotron to the Teflon disc. The calculated VSWR of the Teflon disc was 1.5:1. Over slightly more than a wavelength, the power in the waterload varied by approximately $\sim 7.7\%$, the power in mode filter #1 varied 15.2% and the power in mode filter #2 varied 29.1%. However, total output power from the gyrotron varied only 5%.

It is reasonable to conclude that the VSWR from the Teflon disc did not significantly alter gyrotron operation. The distribution of power in the mode filters and the waterload did change somewhat due to changing line length. An important consideration in interpreting the results of these tests is that the operating frequency of the gyrotron varied slightly (approximately 7 MHz) with each length change due to the impedance variation of the load.

B. Tube 7R1

This tube, which had been successfully operating at 50 kW CW at Oak Ridge since December, abruptly ceased to operate in March. The problem was traced to an open heater in the cathode assembly. The tube was returned to Varian, Palo Alto where the cause of this failure will be investigated.

C. Tube 12(M)

Tube #12(M) is identical to tube #7 with the exception that its loaded Q is approximately 500; #7 has a Q of 750. Effort on this tube was increased in order to provide a suitable backup for tube #7 at Oak Ridge.

Several iterations were made in cold test to optimize the spacing between cavity and miter assembly to lower the Q to 500 in order to achieve improved efficiency at higher beam current.

Some reflection was noted in the output waveguide and was improved by modifying the taper angle on the window taper assembly.

The tube was processed and tested in the pulse mode up to 130 kW peak power at 8% duty where it operated for more than 10 hours. Efficiency versus beam current was found to range from 22 to 34%. (Figure 11.) To determine what fraction of the output power of Tube 12M is circular electric mode, a series of mode filter tests were conducted. Two mode filters were installed between the gyrotron and a miter-bend followed by a waterload (Figure 10C). In order to interpret the experimental data, the following assumptions were made: (1) the two mode filters have identical

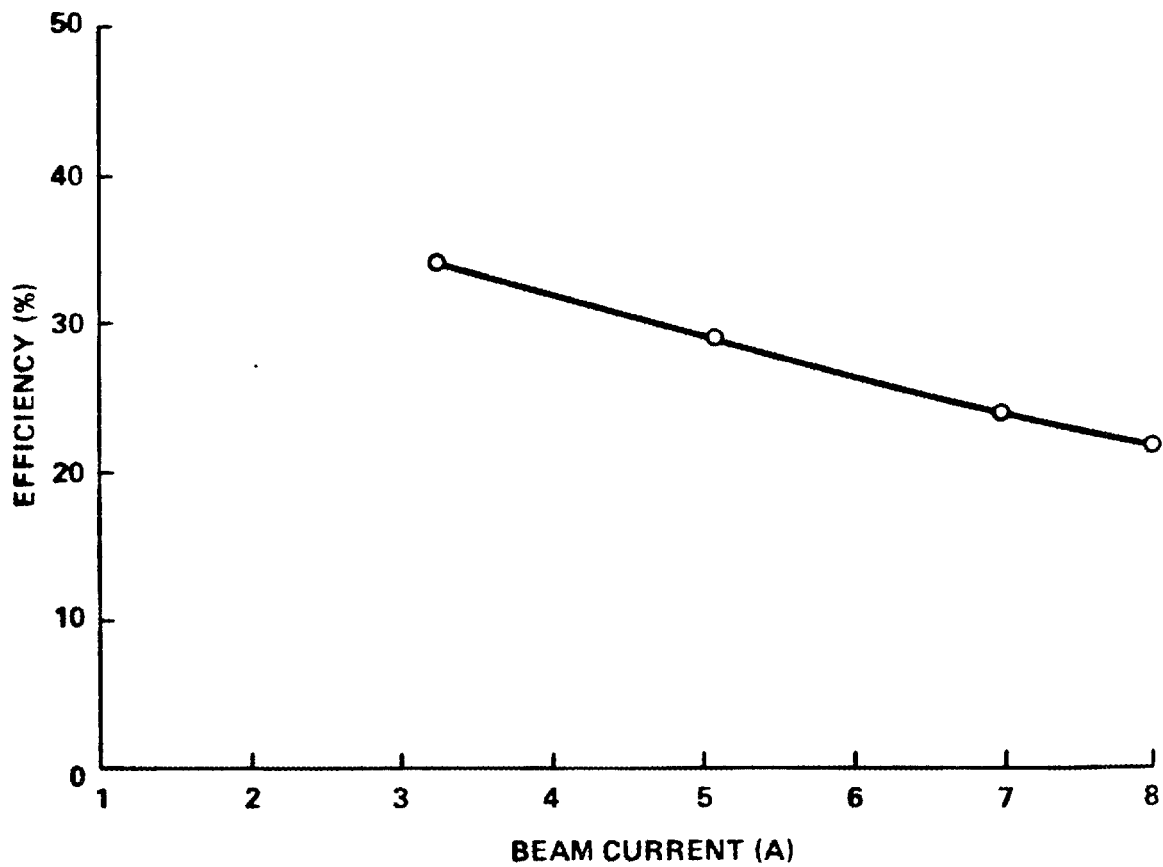


FIGURE 11. VGA-8000 GYROTRON, S/N 12 EFFICIENCY VS BEAM CURRENT IN PULSE MODE, 8% DUTY

characteristics; (2) the miter-bend following the filters does not greatly affect the power absorbed by the mode filters.

Although the second assumption may not be correct, it is a reasonable assumption in order to gain some idea of the mode content of tube 12M.

From the test results, the power absorbed in the mode filter closest to the gyrotron was between 15.7% and 29.9%. The power absorbed in the mode filter near the miter-bend was between 6.2% and 9.4%. The wide variation in power absorbed is a combined result of gyrotron operating parameters and mode filter absorption characteristics. It was concluded that the noncircular electric mode content of tube 12M varied from 29.6% to 44% and the attenuation of a mode filter in one direction varied from 3 dB to 6.3 dB (mean value 4.7 dB).

The tube was then operated at 60 kW CW in excess of 10 hours. Some collector seal heating was noted and was minimized by careful adjustment of the main magnet coil currents.

After consultation with Oak Ridge, the tube was operated between 103 and 113 kW for over one hour. The limiting factor on maximum power was the collector seal temperature rise. The maximum temperature recorded on the four thermocouples located on the collector seal was 59.5°C and the lowest temperature reading was 31.5°C. Table 2 is a summary of the final test performance and the related major parameter values.

Table 2
VGA-8000 S/N 12M Test Performance

OPERATING PARAMETERS

Collector Water Flow	274 gpm
Body Water Flow	3.8 gpm
Window Water Flow (both)	1 gpm
FC-75 Flow	3.0 gpm
Upper Water Load	1.8 gpm
Magnet Coil Currents:	Main 1 = A 500
	2 = A 480
	3 = A 479
	4 = A 469
	Gun 1 = 10.5 A
	2 = 10 A
Beam Voltage	80.5 kV
Gun Anode Voltage	20.1 kV
Cathode Current	5.9 A
Body Current	20.0 mA
Power Output	107 kW
Frequency	27.991 GHz

The tube was shipped to Oak Ridge on March 18, and installation was begun on March 19th. Operation was halted because of work required on the power supply. Installation is tentatively planned to be continued the week beginning April 7th.

D. Tube #6

This tube is a 2 1/2" axisymmetric tube identical to tube #5, except for a new collector seal design, elimination of the window insulator, and a BeO output window. This tube is ready for final assembly except for the collector seal. It has been extensively used for cold test work in response to improvements indicated by the testing of tube #5.

The pacing item on #6 is the new collector seal design. The present design incorporates a rubber water seal. The improved design now being fabricated is made completely from metal and ceramic and should be more reliable and able to withstand higher pressures. Difficulty is being encountered in final assembly of the device as evidenced by cracking of the ceramic. The design has been modified to permit more stress relief in the ceramic and associated structure.

A consultant has investigated possible changes in the cavity window design to eliminate or minimize the problem of higher frequency modes at turn-on and the 26.8 GHz mode sometimes observed at high power. As a result of his input, a new cold test cavity has been constructed and preliminary results obtained. The cavity has been tested and machined to further optimize its geometry. At this point, the unwanted modes have been shifted further away from the operating frequency but new frequencies have appeared. These will be investigated further and identified.

A BeO window is planned for this tube in contrast to the alumina window in #5. This is being done to determine if the greater bandwidth of the BeO window will provide better loading for unwanted modes. The dissipation of the BeO window will be somewhat higher than in the alumina window.

E. Tubes #9 & 10

Because of the successful achievement of 200 kW CW on the 2 1/2" axisymmetric tube in February, this effort has been halted. The main thrust of the 28 GHz gyrotron program will be on the 2 1/2" axisymmetric tube.

F. Tubes #8 & 11

These are 2 1/2" axisymmetric tubes identical to tube #6, except for possible improvements which may be indicated by tubes #5 and #6.

The cooling water system will be redesigned and a shroud placed over the outside to simplify the plumbing connections and improve the tube's appearance.

III. PROGRAM SCHEDULE AND PLANS

With the shipment of tube serial #12 to Oak Ridge in March, and the discontinuation of the effort on the 5" tubes 9 & 10, all remaining effort will be devoted to the four 2 1/2" axisymmetric tubes #'s 5, 6, 8, and 11 described earlier in this report.

It is planned to ship #5 immediately following the CW mode filter and miter-bend tests.

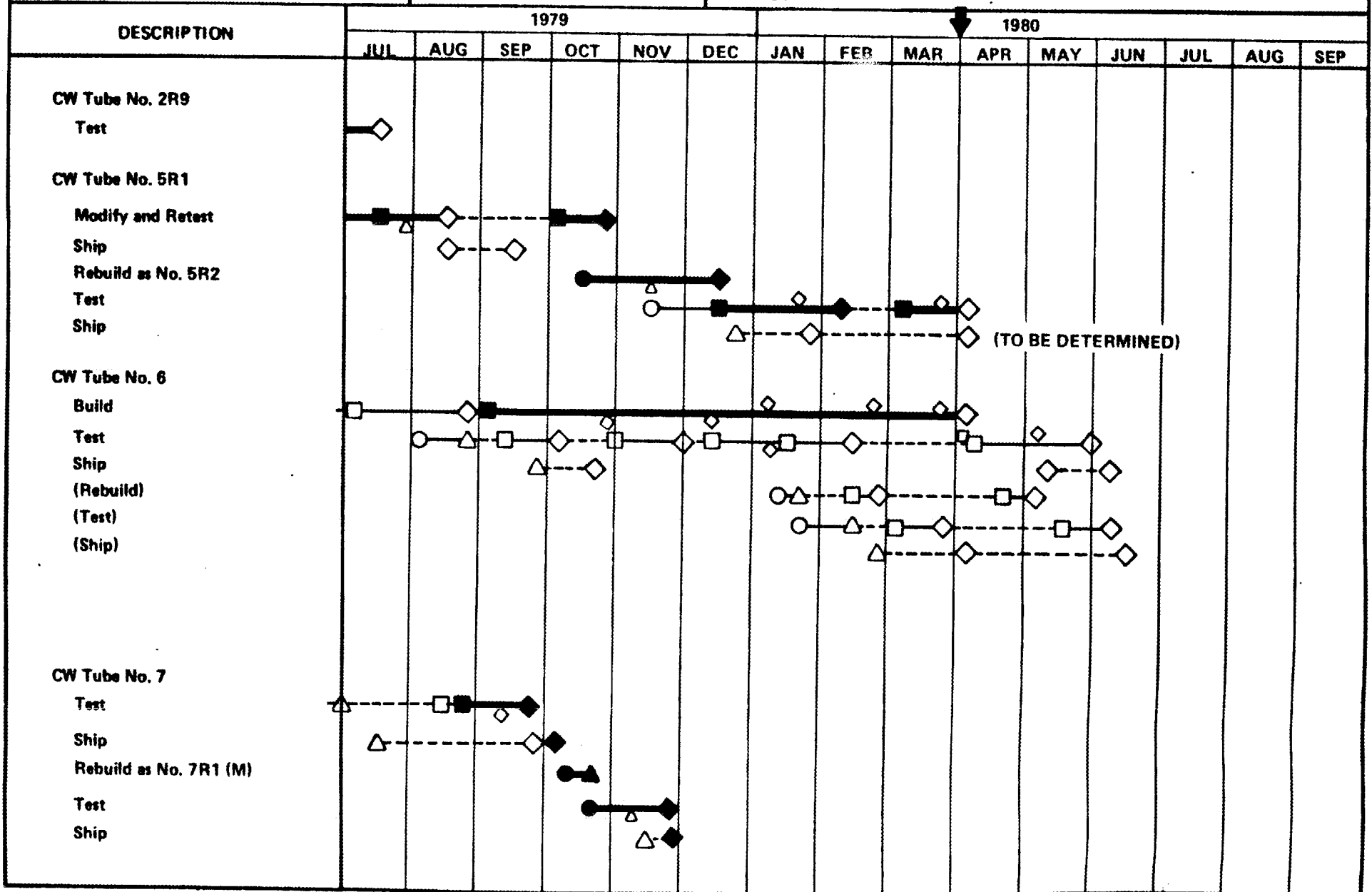
MILESTONE CHART AND STATUS REPORT

- ORIGINAL START
- REVISED START
- △ MAJOR MILESTONE
- ▽ INTERMEDIATE OR DECISION POINT
- ◇ PROPOSED SCHEDULED DEVIATION FOR A MAJOR MILESTONE
- ↓ STATUS REPORT TIME
- ACTIVITY SCHEDULED
- ▬ ACTIVITY COMPLETED

PROGRAM **200 kW, CW, 28 GHz;
DEVELOPMENT**

JOB NO.

STATUS REPORT DATE
31 MARCH 1980



(TO BE DETERMINED)

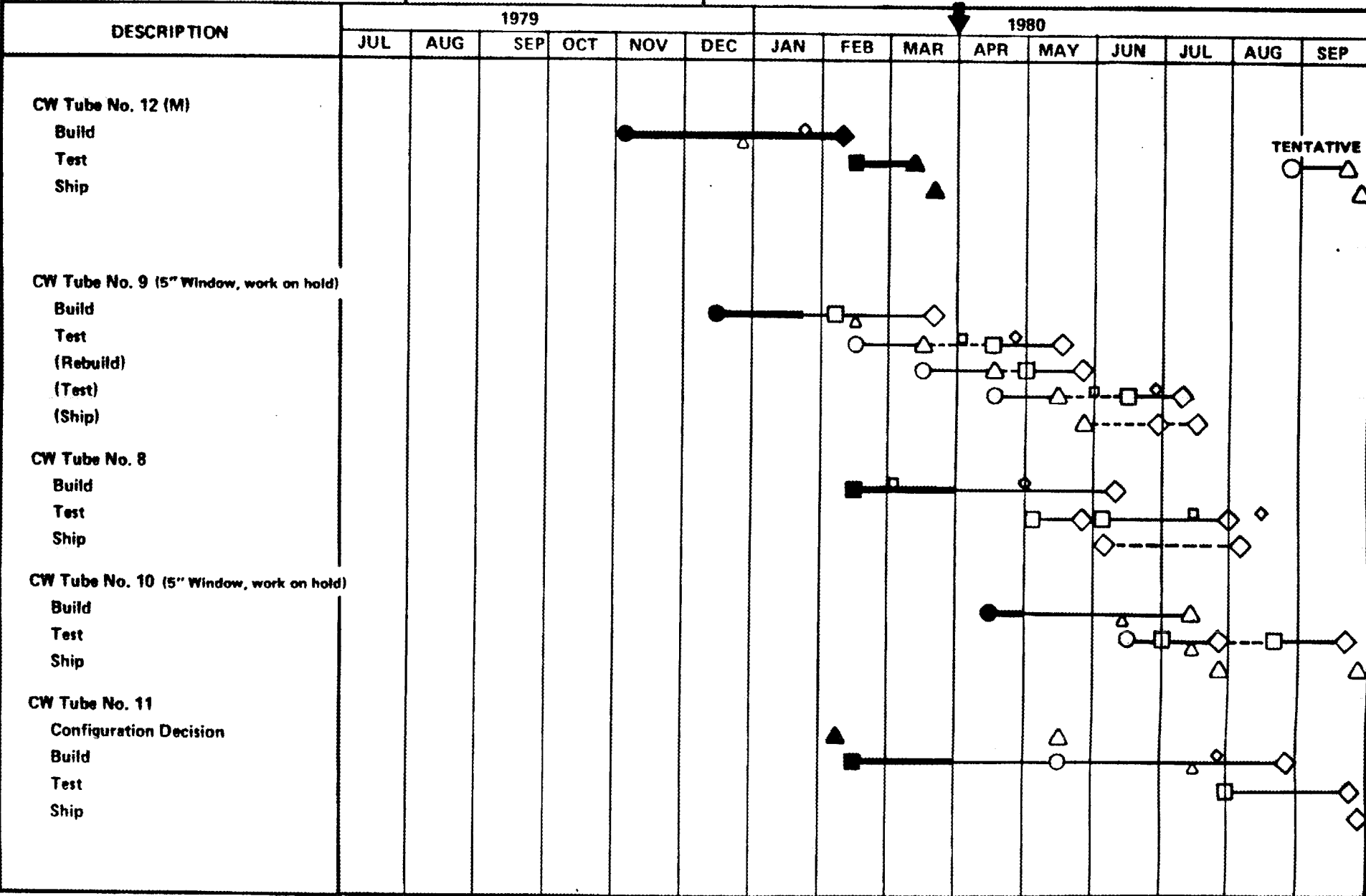
MILESTONE CHART AND STATUS REPORT

- ORIGINAL START
- REVISED START
- △ MAJOR MILESTONE
- ▽ INTERMEDIATE OR DECISION POINT
- ◇ PROPOSED SCHEDULED DEVIATION FOR A MAJOR MILESTONE
- ↓ STATUS REPORT TIME
- ACTIVITY SCHEDULED
- ACTIVITY COMPLETED

PROGRAM **200 kW, CW, 28 GHz;
DEVELOPMENT**

JOB NO.

STATUS REPORT DATE
31 MARCH 1980



TENTATIVE

IV. REFERENCES

1. H.R. Jory, E.L. Lien, and R.S. Symons, "Final Report, Millimeter Wave Study Program" Oak Ridge National Library Order No. Y-12 11Y-49438V, November 1975.
2. V.A. Flyagin et al, "The Gyrotron", Trans MTT, Vol. 25 No. 6 pp 514-521, June 1977.
3. J.L. Hirshfield and V.L. Granatstein, "The Cyclotron Resonance Maser - An Historical Survey", *ibid* pp 522 - 527.
4. S. Hegji, et al, Quarterly Report No. 6, "Development Program for a 200 kW, CW, 28 GHz Gyroklystron", Union Carbide Contract No. 53X01617C, Varian Associates, Inc., pp 115 - 127, July through September 1977.

ORNL/SUB-01617C
5/5/80

INTERNAL DISTRIBUTION

- | | |
|-----------------------|--|
| 1. L. A. Berry | 16. G. F. Pierce |
| 2. A. L. Boch | 17. T. L. White |
| 3. J. L. Burke | 18-19. Laboratory Records Department |
| 4. R. J. Colchin | 20. Laboratory Records, ORNL-RC |
| 5-8. H. O. Eason | 21. Y-12 Document Reference Section |
| 9. D. C. Eldridge | 22-23. Central Research Library |
| 10. R. P. Jernigan | 24. Fusion Energy Division Library |
| 11-13. C. M. Loring | 25. Fusion Energy Division Communications Center |
| 14. H. C. McCurdy | 26. ORNL Patent Office |
| 15. O. B. Morgan, Jr. | |

EXTERNAL DISTRIBUTION

27. R. A. Dandl, 1122 Calle De Los Serranos, San Marcos, CA 92069
28. A. N. Dellis, Culham Laboratory, Abingdon, Oxon, England, OX143DB
29. W. P. Ernst, Princeton University, Plasma Physics Laboratory, P.O. Box 451, Princeton, NJ 08540
30. W. Friz, AFAL/DHM, Wright Patterson AFB, OH 45433
31. T. Godlove, Particle Beam Program, Office of Inertial Fusion, Department of Energy, Mail Stop C-404, Washington, DC 20545
32. V. L. Granatstein, Naval Research Laboratory, Code 6740, Washington, DC 20375
33. G. M. Haas, Component Development Branch, Office of Fusion Energy (ETM), Department of Energy, Mail Stop G-234, Washington, DC 20545
34. J. L. Hirshfield, Yale University, Department of Engineering and Applied Science, P.O. Box 2159, Yale Station, New Haven, CT 06520
35. H. Ikegami, Institute of Plasma Physics, Nagoya University, Nagoya 464, Japan
36. J. V. Lebacqz, Stanford Linear Accelerator Center, P.O. Box 4349, Stanford, CA 94305
37. K. G. Moses, TRW Defense & Space Systems, 1 Space Park, Bldg. R-1, Redondo Beach, CA 90278
38. M. R. Murphy, Office of Fusion Energy (ETM), Department of Energy, Mail Stop G-234, Washington, DC 20545
39. V. B. Napper, Three Dunwoody Park, Suite 112, Atlanta, GA 30341
40. B. H. Quon, TRW Defense & Space Systems, 1 Space Park, Bldg. R-1, Redondo Beach, CA 90278
41. M. E. Read, Naval Research Laboratory, Code 6740, Washington, DC 20375
42. D. B. Rensen, General Atomic Company, P.O. Box 81608, San Diego, CA 92138
43. B. Stallard, Lawrence Livermore Laboratory, University of California, L-437, P.O. Box 808, Livermore, CA 94550
44. H. S. Staten, Office of Fusion Energy (ETM), Department of Energy, Mail Stop G-234, Washington, DC 20545
45. P. Tallerico, AT-1, Accelerator Technology Division, Los Alamos Scientific Laboratory, Mail Stop 817, P.O. Box 1663, Los Alamos, NM 87545
46. J. J. Tancredi, Hughes Aircraft Company, Electron Dynamics Division, 3100 W. Lomita Blvd., Torrance, CA 90509
47. R. J. Tenkin, National Magnet Laboratory, Massachusetts Institute of Technology, Cambridge, MA 02139

ORNL/SUB-01617C
5/5/80

EXTERNAL DISTRIBUTION (continued)

48. A. Triveipiece, Science Applications, Inc., 1200 Prospect Street, P.O. Box 2351, LaJolla, CA 92038
49. Director, U.S. Army Ballistic Missile Defense Advance Technology Center, Attn.: D. Schenk, ATC-R, P.O. Box 1500 Huntsville, AL 35807
- 50-51. Department of Energy Technical Information Center, Oak Ridge, TN 37830
52. RADC/OCTP, Griffiss AFB, NY 13441
53. System Manager for Energy Research and Development, Oak Ridge Operations Office, Department of Energy, Oak Ridge, TN 37830